

14 Mar 1991, 10:30 am - 12:30 pm

## Pore Pressure Response During 1986 Lotung Earthquakes

C. K. Shen  
*University of California, Davis, CA*

Zhiliang Wang  
*Geomatrix Consultants, San Francisco, CA*

X. S. Li  
*University of California, Davis, CA*

Follow this and additional works at: <https://scholarsmine.mst.edu/icrageesd>



Part of the [Geotechnical Engineering Commons](#)

### Recommended Citation

Shen, C. K.; Wang, Zhiliang; and Li, X. S., "Pore Pressure Response During 1986 Lotung Earthquakes" (1991). *International Conferences on Recent Advances in Geotechnical Earthquake Engineering and Soil Dynamics*. 39.

<https://scholarsmine.mst.edu/icrageesd/02icrageesd/session03/39>



This work is licensed under a [Creative Commons Attribution-Noncommercial-No Derivative Works 4.0 License](#).

This Article - Conference proceedings is brought to you for free and open access by Scholars' Mine. It has been accepted for inclusion in International Conferences on Recent Advances in Geotechnical Earthquake Engineering and Soil Dynamics by an authorized administrator of Scholars' Mine. This work is protected by U. S. Copyright Law. Unauthorized use including reproduction for redistribution requires the permission of the copyright holder. For more information, please contact [scholarsmine@mst.edu](mailto:scholarsmine@mst.edu).



## Pore Pressure Response During 1986 Lotung Earthquakes

C.K. Shen

Professor of Civil Engineering, University of California, Davis

X.S. Li

Associate Development Engineer, University of California, Davis

Zhiliang Wang

Senior Staff Engineer, Geomatrix Consultants, San Francisco, CA

**SYNOPSIS:** In 1986, two significant earthquake events in Lotung, Taiwan were recorded with both acceleration and pore water pressure traces at different depths below the ground surface. One event ( $M=6.2$ ) was recorded on July 30th with an epicentral distance of 6km, and the other ( $M=7.0$ ) was recorded on November 14th with an epicentral distance of about 80 km from the site. To analyze the recorded data, a finite element procedure was developed. The procedure incorporates a newly developed bounding surface hypoplasticity model for granular soils and can handle multidirectional input motions. The finite element procedure takes into consideration pore water pressure buildup and dissipation, pore water movement relative to the soil skeleton, compressibility of pore water, initial values of  $k_0$ , overconsolidation ratios, and rotational shear effects. This paper describes the field project and presents the analytical results based on the above procedure which include the multidirectional shaking effects. The analytical results compare well with the field measurements.

### INTRODUCTION

The October 1989 Loma Prieta Earthquake vividly demonstrated the vast destructive power of seismic events and how soil liquefaction contributed to damages of buildings, roadways, docks, bridges, utility lines, and others. For a saturated granular soil deposit, ground movement due to earthquake motion is often preceded by the buildup of excess pore water pressure in the soil. The amount of pore water pressure buildup thus has a direct bearing on the response of the soil during an earthquake.

In recent years there has been a growing consensus among geotechnical as well as earthquake engineers that major efforts should be given to establishing a broad field data base for close examination of analytical and empirical methods for prediction of dynamic response of granular soils under earthquake loadings. Such an undertaking is important because it provides a unique opportunity to evaluate our capabilities in earthquake response predictions. Field pore water pressure response measurements have been reported by Ishihara (4,5). Bennett, et al., (1), and Holzer, et al., (3).

### THE LOTUNG PROJECT

Since 1984, the Electric Power Research Institute (EPRI) of Palo Alto, California and the Taiwan Power Company (TPC) have jointly established a seismic model study site located in Lotung, Taiwan. A scaled model of a nuclear containment structure was built and instrumented with the purpose of studying the soil-structure interaction and the dynamic response of the nuclear containment structure under earthquake loadings. As a part of the research project, the installation and monitoring of pore water pressure response was jointly carried out by the University of California, Davis, and the National Taiwan University.

The layout of the site instrumentation is shown in Fig. 1. In the figure the 1/4 scale model is a scaled-down reinforced concrete water reactor containment structure. Among the various instruments, the acceleration network, centered around the model, consisted of three surface (ARM-1, -2 and -3) and two downhole (DHA and DHB) arrays. The surface arrays, intersecting at the center of the model, were approximately  $120^\circ$  apart from each other. The downhole arrays located along ARM-1 array, extended to a depth of 50 meters. Triaxial accelerometer sets were installed at the ground surface and at depths of 6, 11, 17 and 47 meters. The pore water pressure transducers were embedded in clusters at locations along the accelerometer arrays. Since potentially liquefiable soil layers were found between 2 ~ 20 meters below the ground surface, the transducers were positioned at depths between 3 to 16 meters from the surface. Also shown in Fig. 1 are the

locations of transducers. For a detailed description of the pore pressure sensors and the recording network, the readers are referred to reference 2.

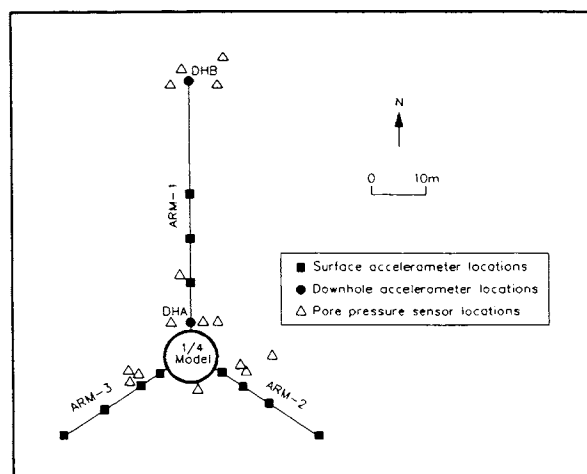


Fig. 1 Locations of accelerometers and pore pressure transducers

### BRIEF DESCRIPTION OF THE SITE CONDITION

A total of 8 bore holes (L1-L8) were drilled on the site, their locations are shown in Fig. 2. The depths of the bore holes were 60 m, except for the B.H. L5 which was drilled to a depth of 150 m. Extensive field and laboratory tests were performed and reported elsewhere. (9,10,11,15,16).

Based on the boring log information and laboratory physical property test results, generalized soil profiles, Section A-A, (B.H., L1, L3 and L4) and Section B-B (B.H. L2, L7 and L3) are presented in Figs. 3 and 4, respectively. Also shown in the Figures are the  $N$ -values and field water contents ( $w\%$ ) vs. depths. At depths of approximately 34 m and greater, the soil is a greyish silty clay, relatively firm with medium plasticity. Above that there are interbedded layers of clayey silts and silty sands. Relatively low  $N$ -values and densities are found in layers at shallower depths (up to approximately 20 m below the ground surface); these layers are potentially susceptible to liquefaction or loss of strength during earthquakes. For this reason, all the pore

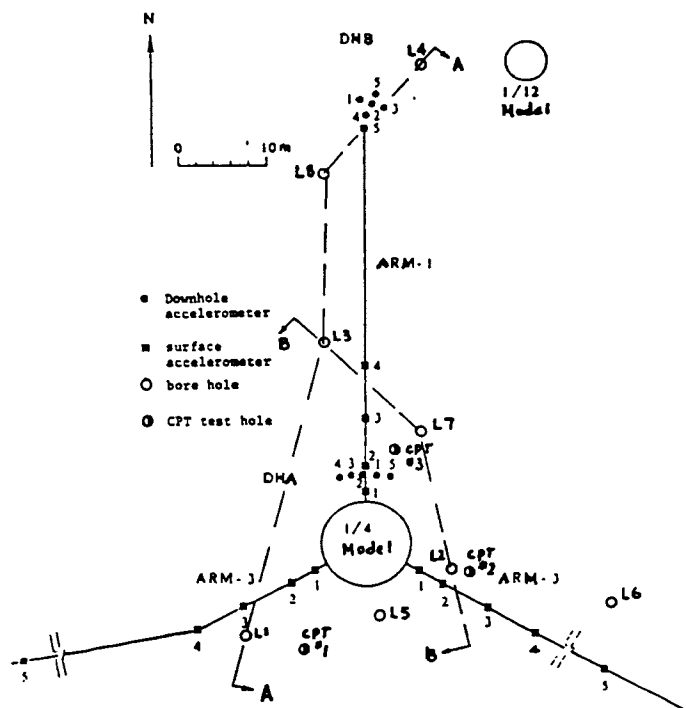


Fig. 2 Site investigation and instrumentation plan

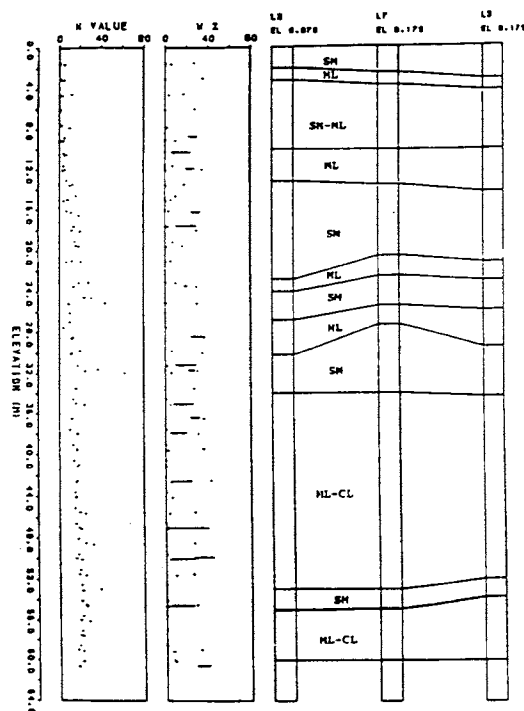


Fig. 4 Soil profile, N-value, water content (Section B-B)

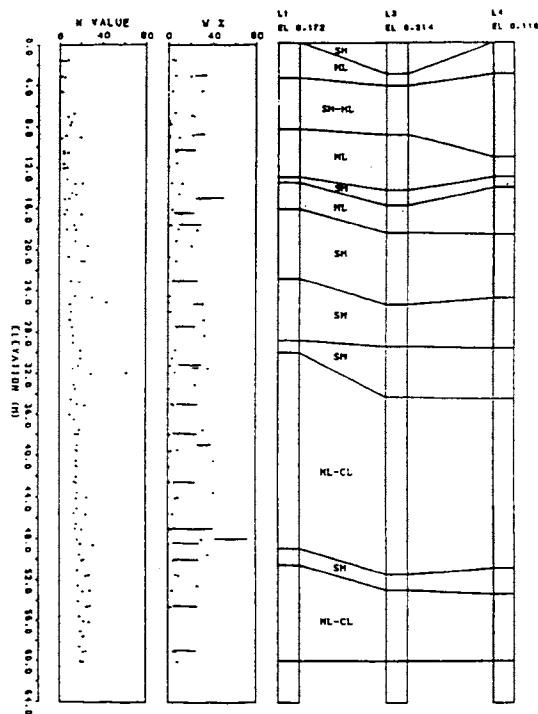


Fig. 3 Soil profile, N-value, water content (Section A-A)

pressure sensors are installed in this region. More specifically, the surface in general is covered by a 0.5 to 3 m thick sandy, silty fill with occasional gravels, pebbles, and wood chips. A low plasticity greyish clayey silt layer is located 2 to 4 m below the ground surface. This is a weak and compressible recent deposit of relatively low permeability. Located between 3 and 9 m below the surface (11 m towards the north end of the site) is a layer of black, silty fine sand with thin lenses of

grey clayey silt. From 9 to 14 m is another layer of greyish clayey silt similar to the one located just below the fill. The last layer in the upper 20 m is a relatively dense silty sand deposit. Since the black, silty fine sand is a loose deposit located between two relatively impervious clayey silt layers, it appears to have the most potential to liquefy under earthquake loadings.

It is also interesting to note that there exists an artesian pressure head on the site. The static ground water level before penetrating the artesian layer is about 0.5 m below the ground surface. The artesian pressure is found in the silty fine sand layer at approximately 7-8 m depth. The full artesian pressure head would cause the water level to rise approximately 1 to 1.5 m above the ground surface.

### PORE PRESSURE RECORDS

Since the installation of the pore pressure sensors in late May of 1986, two strong earthquakes originating off-shore from the eastern coast of Taiwan have been recorded. The epicenter of the July 30, 1986 earthquake ( $M = 6.2$ ) was located about 6 km from the site; whereas, the epicentral distance of the November 15, 1986 earthquake ( $M = 7.0$ ) was about 80 km. A total of 16 response records were registered. The two major earthquakes took place within a time span of less than 4 months. In each instance, the maximum induced pore water pressure rise was less than 30% of the effective overburden pressure and on the site, no settlement of the ground or the model structures could be visually detected. The November earthquake was the largest in Taiwan since 1978 (Nov. 15, 1986; 05:20 a.m.; Epicenter  $E 121^{\circ} 50, 17'$ ;  $N 23^{\circ} 57.65'$ ; focal depth 6 km;  $M = 7.0$ ). Severe damages were reported in Taipei, Hualien, Lotung, and Ilan areas, while the July earthquake was more localized (July 30, 1986; 19:31 p.m.; Epicenter:  $E 121^{\circ} 47.65'$ ,  $N 24^{\circ} 37.73'$ ; focal depth: 1.6 km;  $M = 6.2$ ). It was felt mostly in the Lotung-Ilan area. According to information given by the Taiwan Provincial Weather Bureau, the intensity of ground shaking in Lotung area was the same for both earthquakes; the pore water pressure response records from the two earthquakes were however quite different. This is due probably to the differences in epicentral distance, focal depth, duration of shaking, etc. Tables 1 and 2 tabulate the recorded pore water pressure rise and fall during the July and November earthquakes, respectively. It should be noted that the % of pore water pressure rise during earthquake is higher if the artesian conditions are considered.

TABLE 1. Pore Pressure Response - July Earthquake

Sensor No.	Channel No.	Depth, h (m)	Hydrostatic Pressure $u_0$ (ksc)	Max Induced Pore Pressure $\Delta u$ (ksc)	$\Delta \gamma' h$ (ksc)	Gradient $\frac{u_0 - h}{\gamma' h}$	Effective Overburden Pressure (ksc) $\sigma_v' = \Sigma \sigma_v' h - 1 \gamma_w h$	$R = \frac{\Delta u}{\sigma_v' T}$ (%)	$R' = \frac{\Delta u}{\sigma_v' T'}$ (%)	Time to Reach $\Delta u$ (sec)	Time to Dissipate 50% $\Delta u$ (sec)
PA-1	1	5.06	0.560	0.052	0.573	0.107	0.519	10.0	9.2	24	138
PF-1	5	3.25	0.335	0.061	0.267	0.030	0.257	23.7	22.9	5	9
PF-2	6	6.05	0.568	0.022	0.522	-	0.522	4.2	4.2	4	4
PF-5	9	12.00	1.245	0.040	1.259	0.038	1.214	3.3	3.2	9	-*
PN1-0	11	3.16	0.406	0.022	0.335	0.285	0.245	9.0	6.7	7	3
PN1-1	12	6.03	0.628	0.160	0.623	0.040	0.598	26.8	25.8	5	21
PN1-4	15	5.53	0.638	0.031	0.614	0.154	0.529	5.9	5.1	14	?
PN2-1	18	6.30	0.635	0.105	0.651	0.008	0.646	16.3	16.1	5	207
PA-3'	21	5.10	0.573	0.098	0.576	0.124	0.513	19.1	17.2	3	2
PN3-1	24	6.38	0.743	0.081	0.658	0.165	0.553	14.6	12.4	3	35
PN3-2	29	11.00	1.193	0.040	1.086	0.085	0.993	4.0	3.7	9	93

\* Time to dissipate 50%  $\Delta u$  was longer than the period of recording.

R is the stress ratio considering artesian effect.

R' is the stress ratio without considering artesian effect where  $\sigma_v' = \Delta \gamma' h$ .

TABLE 2. Pore Pressure Response - November Earthquake

Sensor No.	Channel No.	Depth, h (m)	Hydrostatic Pressure $u_0$ (ksc)	Max Induced Pore Pressure $\Delta u$ (ksc)	$\Delta \gamma' h$ (ksc)	Gradient $\frac{u_0 - h}{\gamma' h}$	Effective Overburden Pressure (ksc) $\sigma_v' = \Sigma \sigma_v' h - 1 \gamma_w h$	$R = \frac{\Delta u}{\sigma_v' T}$ (%)	$R' = \frac{\Delta u}{\sigma_v' T'}$ (%)	Time to Reach $\Delta u$ (sec)	Time to Dissipate 50% $\Delta u$ (sec)
PF-8	17	15.00	1.270	0.115	1.622	-	1.622	9.3	9.3	18	30
PN2-1	18	6.30	0.684	0.156	0.651	0.086	0.597	26.1	24.2	24	207
PA-3'	21	5.10	0.575	0.117	0.576	0.127	0.511	22.9	20.5	18	86
PN2-2'	23	8.00	1.211	0.052	0.811	0.514	0.400	13.0	6.7	22	-*
PN3-1	24	6.38	0.820	0.102	0.658	0.285	0.477	21.4	16.0	21	69

\* Time to dissipate 50%  $\Delta u$  was longer than the period of recording.

R is the stress ratio considering artesian effect.

R' is the stress ratio without considering artesian effect where  $\sigma_v' = \Delta \gamma' h$ .

Referring to Tables 1 and 2, sensors PN1-1, PN2-1 and PN3-1 (Channels 12, 18 and 24) were placed approximately at the same depth (6 m) in the same soil layer (SM). Their distances to the rim of the foundation of the main structure vary from approximately 2 to 6 m. For the July earthquake it is shown in all three records that the maximum pore water pressure increase occurred at about 3 to 5 seconds into the recording with a registered maximum pore pressure increase ranging from 27% to 15% of their respective effective overburden pressure. The time for a 50% dissipation of the induced pore pressure varied from 21 to 207 seconds. Furthermore, examples of the pore pressure response recorded for sensors placed in the same soil deposit at more or less the same depth during the July and November earthquakes are shown in Figs. 5a and Figs. 6a and b, respectively. Note the differences in the magnitude of excess pore pressure buildup and the rate of its dissipation. The above information reveals that field pore pressure response measurements can be affected significantly by local soil conditions, hence variations and similarities in response from different sensors as those cited can perhaps be expected in most cases. Consequently, when field pore pressure response records are examined or studied, it seems that more attention should be paid to the general trend of the response and not necessarily the response of a specific record.

#### PORE WATER PREDICTION

A recently developed finite element procedure to analyze the response of stratified level grounds under multidirectional earthquake loading conditions (6), was used for the Lotung site response study. The

procedure performs nonlinear effective-stress-based analysis under true three directional earthquake loading conditions. The procedure takes into consideration pore water pressure buildup and dissipation, pore water movement relative to the soil skeleton, compressibility of pore water, initial values of  $k_0$ , and rotational shear effects. Because of its multidirectional nature, the procedure can handle both shear wave and compression wave simultaneously and predict not only pore pressure response and horizontal motion but also permanent settlement. There are three constitutive models built into the procedure: an elastic model for elastically behaved soils (e.g. the soils in very deep layers); a hypoplasticity model for granular materials; and a bounding surface clay model for cohesive soils. Among them the model for granular materials (13) is particularly interesting. The model, formulated within the general framework of bounding surface concept, can simulate the behavior of granular soils under a variety of loading conditions. In contrast to classical plasticity, the model yields plastic volumetric strain even under neutral loading paths. Because of this, the model can imitate the behavior of granular soil under a class of loading paths called rotational shear under which the second invariant J of the deviatoric stress tensor is kept constant. It is conceivable that during earthquake soil could experience rotational shear associated loadings, thus a constitutive model capable of properly simulating soil behavior under rotational shear is desirable in analyzing the site response under multidirectional earthquake shaking.

Based on the generalized site soil profile described earlier, a 17 element mesh as shown in Fig. 7 is configured for the analysis. The bottom boundary is located at the depth of 17 m and the downhole

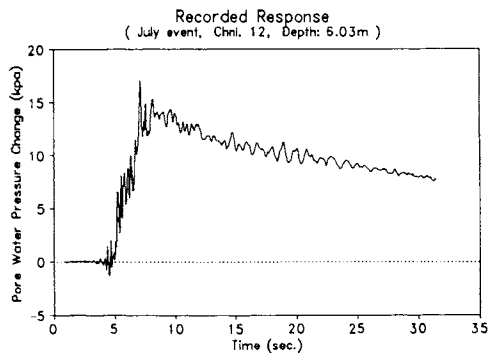


Fig. 5a Pore pressure records of July event, Depth 6m, SM material

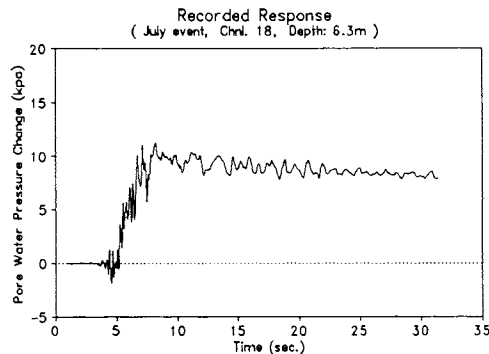


Fig. 5b Pore pressure records of July event, Depth 6.3m, SM material

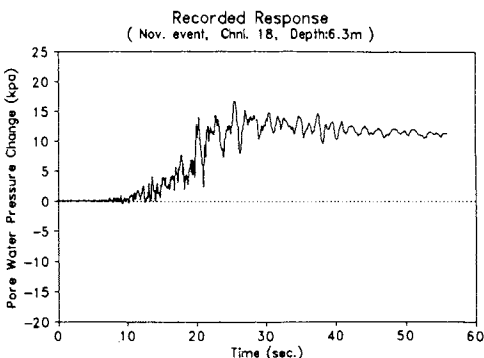


Fig. 6a Pore pressure records of Nov. event, Depth 6.3m, SM material

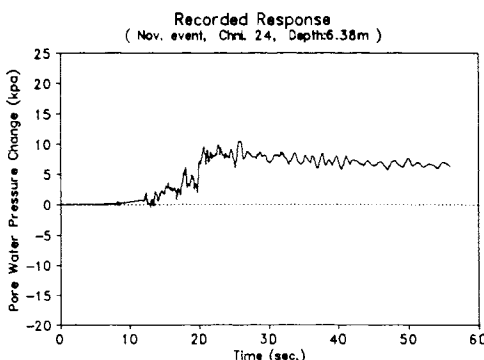


Fig. 6b Pore pressure records of Nov. event, Depth 6.4m, SM material

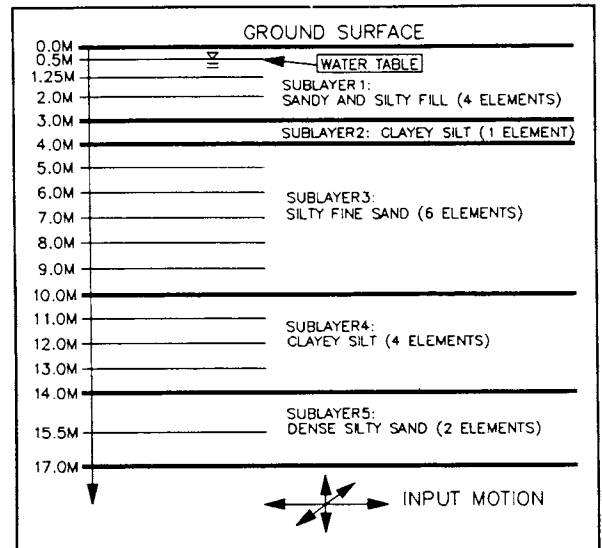


Fig. 7 Soil profile used in analysis

acceleration records at that depth are used as input motions. To define the site specifics, the following additional informations are also needed for each of the elements: the specific gravity of soil solids  $G_s$ , the void ratio  $e_o$ , the coefficient of permeability  $k$ , the undrained bulk modulus  $\Gamma$ , the viscous coefficients  $\eta_s$  and  $\eta_c$ , the  $k_o$  value, the constitutive model type, and the parameters of the constitutive model. Details regarding the determination of these coefficients can be found elsewhere (12).

As shown in Fig. 7, the site basically consists of fine granular materials, therefore the hypoplasticity model is used to represent the soils of all elements in the profile. The current version of the hypoplasticity model has about twenty parameters to be determined to characterize a single material. For each material, a series of laboratory tests performed under specified loading paths was required (14). While in theory it is desirable and possible to have all of the suggested tests performed; in reality however, limited by the quantity of available soil samples, it is not always practical and feasible to perform all of the tests. This is especially true if "undisturbed samples" were required. For the "undisturbed" samples taken from the Lotung site, only a limited number of conventional triaxial and simple shear tests were carried out. While the test results do provide highly valuable information, they are not complete in forming the base for a systematic calibration of all the model parameters. Thus, some of the parameters were determined indirectly. It is generally recognized that the most important property of a granular soil under earthquake loading is its liquefaction potential, therefore it is essential to ensure that the selected model parameters will properly represent the soil's liquefaction resistance. In view of this, cyclic simple shear tests results represented by the stress ratio versus the number of cycles causing initial liquefaction were singled out to be the criterion in choosing model parameters. The triangle marks in Fig. 8 show the isotropically consolidated simple shear results on "undisturbed" samples taken from depths approximately 10 m below the ground surface in sublayers 3 and 4 in Fig. 7. Hence it is assumed that the test results represent the overall liquefaction resistance of the soils in sublayers 2, 3, and 4 (sublayer 2 is included because of the similarity between soils in sublayers 2 and 4). The solid curve in Fig. 8 is obtained from model simulation using selected model parameters. Since similar laboratory results were not available for the first and fifth sublayers, the same fitting process could not be carried out in the manner described above. The liquefaction resistance characteristics of these two layers can only be approximated based on the soil description and the relationship established for sublayers 2, 3 and 4. The curves representing the liquefaction resistances of the two layers are also shown in Fig. 8. They are the results of model simulations with different sets of parameters. The input motions are shown in Figs. 9a through f, they are the three directional ground motion records at 17 m depth for the July and November events, respectively.

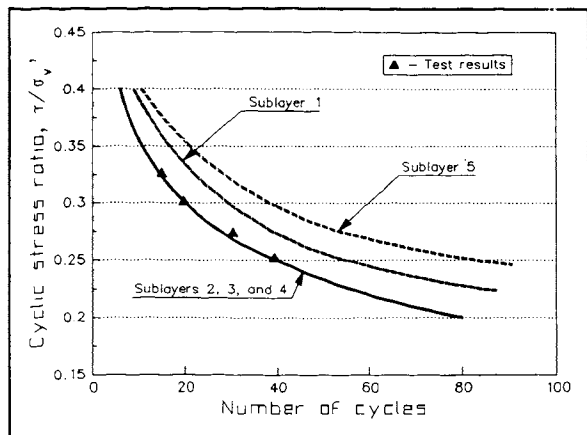


Fig. 8 Liquefaction resistance with assigned parameters

## COMPARISONS & CONCLUSIONS

It should be noted that predicted acceleration along different directions and at different depths compared well with their recorded counterparts (6). Since the paper focuses on pore pressure response only, the acceleration responses will not be elaborated. Eleven pore water pressure traces were recorded during the July event and five during the November event. As noted in Tables 1 and 2 the recorded pore pressure traces differ from location to location, even for the same event and at similar depths. It is believed that the scattering is largely due to the nonuniformity of the soil on the site. In order to make comparison between analysis and measurement possible, the field records at similar depths are grouped as shown in Table 3 and then averaged. The processed averaged traces are shown in Figs. 10 for the July event and 11 for the November event, respectively.

The prediction of pore pressure response at comparable depths are shown in Figs. 10a, b, c, and 11a and b for the July and November events, respectively. It can be seen that, overall, the analytical responses are reasonably agreeable with the field records. The discrepancy between Fig. 10a and Fig. 10d indicates that the

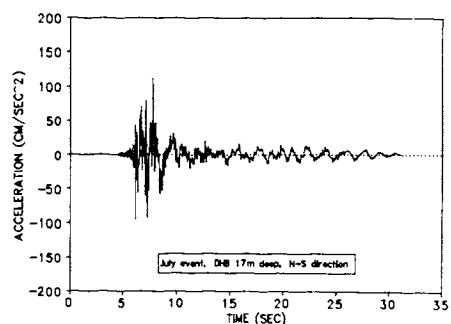


Fig. 9a Input acceleration of July event (Horiz. direction 1)

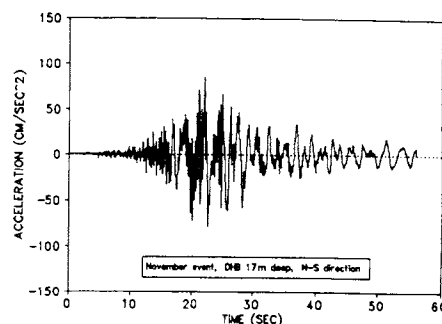


Fig. 9d Input acceleration of November event (Horiz. direction 1)

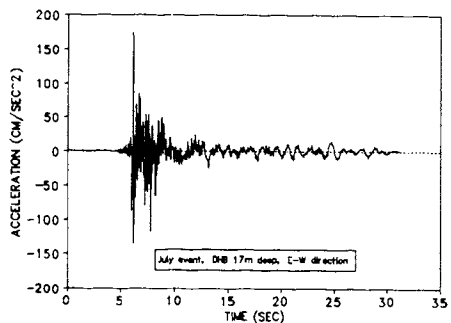


Fig. 9b Input acceleration of July event (Horiz. direction 2)

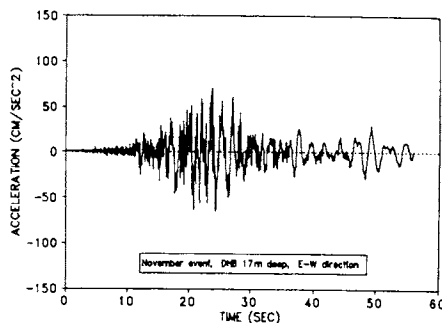


Fig. 9e Input acceleration of November event (Horiz. direction 2)

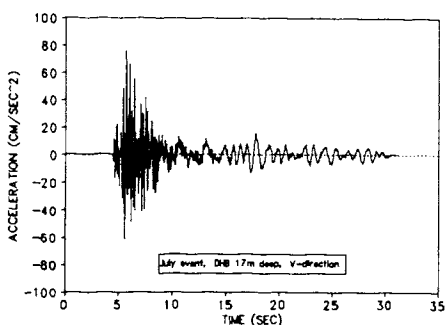


Fig. 9c Input acceleration of July event (vertical direction)

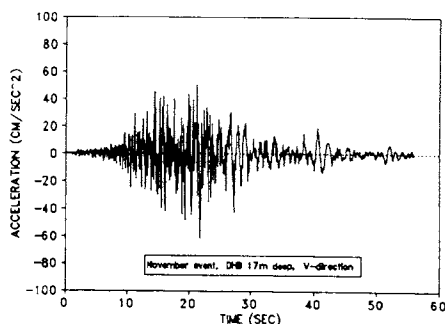


Fig. 9f Input acceleration of November event (vertical direction)

coefficients of permeability estimated for top layers seem a little bit too low. The analytical pore pressure increases shown in Figs. 10c and 11a are also a little bit higher than their recorded counterparts as shown in Figs. 10f and 11c. The somewhat higher excess pore pressure obtained by the analysis implies that the liquefaction resistance of the soils might be slightly underestimated. As mentioned earlier, the liquefaction resistance in the analysis was estimated by matching the response of the constitutive soil model with laboratory simple shear test results on "undisturbed" samples. However, studies (7,8) have shown that even for good quality "undisturbed" samples the cyclic liquefaction resistance

in laboratory tests is often lower than those of in-situ deposits because the effects of prior strain history contributing to the increase in liquefaction resistance is lost to a large extent during sampling and testing preparations. This may explain why some of the analytical excess pore pressures are slightly higher than those measured in the field. Nevertheless, considering the uncertainties involved in the analysis and the limited number of samples of measurement, the difference between analytical and measured pore pressure responses seems insignificant.

As we can see, the July and November earthquakes are two independent events with rather different pore water pressure responses. However, using the same site parameters and different input ground motion records, the analyses yield equally good agreement with their respective averaged field measurements. It should be emphasized that a pore water pressure sensor monitors the response of water pressure at the point of measurement and minor stratifications exist even in relatively uniform soil deposits; thus significant variations in pore pressure response could likely be registered by two sensors located at same depth and only a few meters apart. It is the author's opinion that in studying pore water pressure response records, reliance should not be placed on a single record or two, but rather a large number of records on the site. It should also be noted that the magnitudes of the excess pore water pressure in the Lotung case were relatively low, thus the prediction of liquefaction is yet to be attested. Nonetheless, the

Table 3 Grouped pore water pressure records

Figure No.	Earthquake event	Number of records being averaged	Depths of records being averaged(m)
10d	July	2	3.16, 3.25
10e	July	7	5.06, 5.10, 5.53, 6.03, 6.05, 6.30, 6.38
10f	July	2	10.00, 11.00
11c	November	4	5.10, 6.30, 6.38, 8.00
11d	November	1	15.00

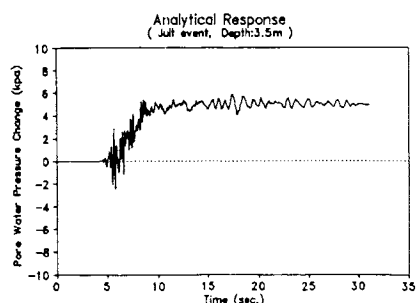


Fig.10a Analytical pore pressure change of July event (Depth: 3.5m)

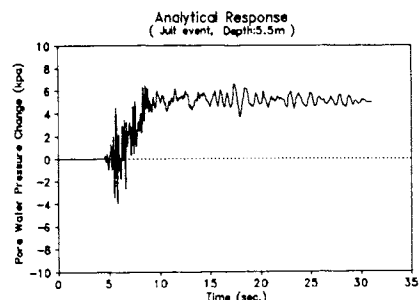


Fig.10b Analytical pore pressure change of July event (Depth: 5.5m)

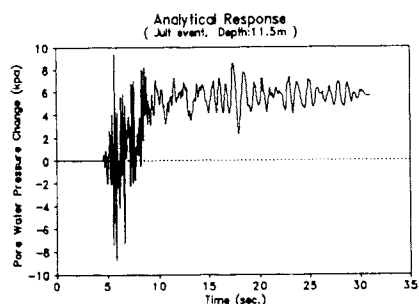


Fig.10c Analytical pore pressure change of July event (Depth: 11.5m)

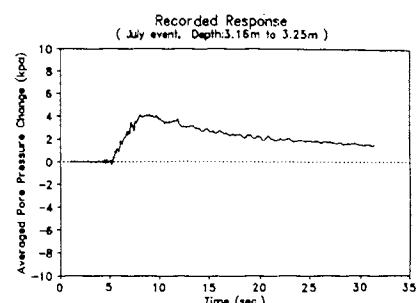


Fig.10d Recorded pore pressure change of July event (averaged from depths of 3.16 to 3.25m)

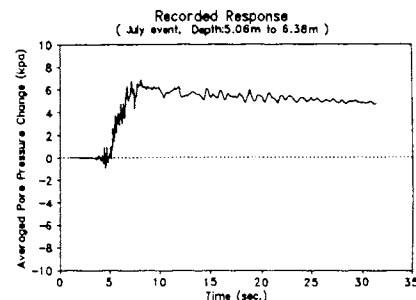


Fig.10e Recorded pore pressure change of July event (averaged from depths of 5.06 to 6.38m)

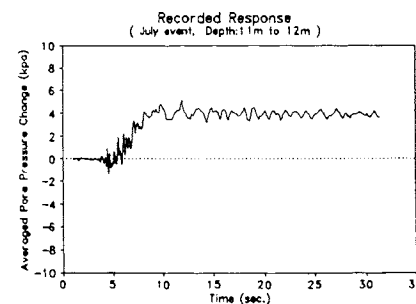


Fig.10f Recorded pore pressure change of July event (averaged from depths of 11 to 12m)

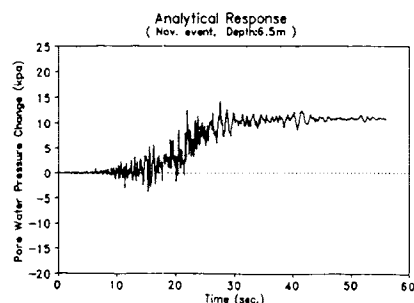


Fig.11a Analytical pore pressure change of November event (Depth: 6.5m)

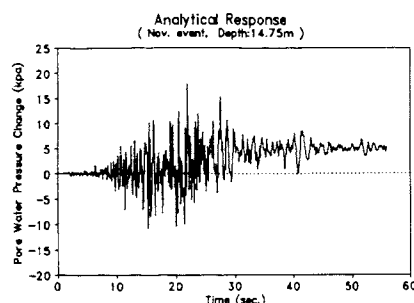


Fig.11b Analytical pore pressure change of November event (Depth: 14.75m)

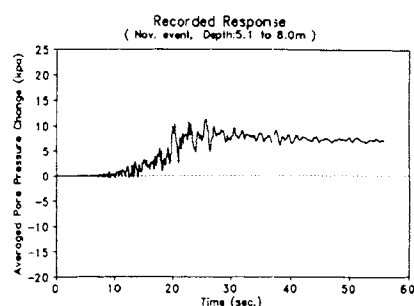


Fig.11c Recorded pore pressure change of Nov. event (averaged from depths of 5.1 to 8.0m)

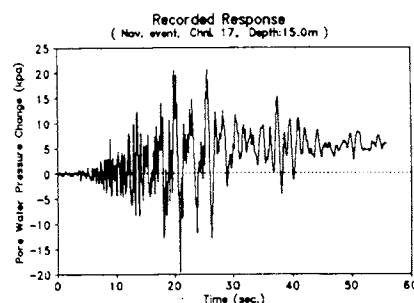


Fig.11d Recorded pore pressure change of Nov. event (Depth: 15.0m)

reasonable agreement between the field data and the predictions of the Lotung project has shown the potential of adopting the procedure for future studies.

#### ACKNOWLEDGEMENTS

The study is sponsored by funds from the National Science Foundation and the Naval Civil Engineering Laboratory. Their support is gratefully appreciated.

#### REFERENCES

Bennett, M.J., P.V. McLaughlin, J.S. Sarmiento, and T.L. Youd (1984), "Geotechnical Investigation of Liquefaction Sites, Imperial Valley, California," Open-File Report 84-252, U.S. Geological Survey, Menlo Park, CA.

Field Pore Water Pressure Response Measurements During Earthquakes (1987), Report to NSF, Department of Civil Engineering, University of California, Davis.

Holzer, T.L., M.J. Bennett, T.L. Youd, and A.T.F. Chen (1986), "Field Investigation to Identify a Site for Monitoring Liquefaction," Cholame Valley, California, Open-File Report 86-346, U.S. Geological Survey, Menlo Park, CA.

Ishihara, K., K. Shimizu, and Y. Yamada (1981), "Pore Water Pressure Measured in Sand Deposits During an Earthquake," *Soils and Foundations*, Vol. 21, No. 4.

Ishihara, K., Y. Anazawa, and J. Kuwano (1987) "Pore Water Pressures and Ground Motions Monitored During the 1985 Chiba-Zbaragi Earthquake," *Soils and Foundations*, Vol. 27, No. 3.

Li, X.S. (1990) "Free Field Soil Response Under Multidirectional Earthquake Loading," Ph.D. Dissertation, Department of Civil Engineering, University of California, Davis.

Seed, H.B. (1976) "Evaluation of Soil Liquefaction Effects on Level Ground During Earthquakes," Liquefaction Problems in Geotechnical Engineering, ASCE National Convention.

Seed, H.B., K. Mori, and C.K. Chan, (1977) "Influence of Seismic History on Liquefaction of Sands," *Journal of the Geotechnical Engineering Division, ASCE*, Vol. 103, No. GT4.

Shen, C.K., X.S. Li, C.K. Chan, T.S. Ueng and C.H. Chen (1987) "In Situ Pore Pressure Measurements During Earthquake," *Proceedings, 2nd International Symposium on Field Measurements in Geomechanics*, Vol. 1, Kobe, Japan.

Shen, C.K., C.K. Chan, X.S. Li, H.W. Yang, T.S. Ueng, W.T. Wu, and C.H. Chen (1989) "Pore Water Pressure Response Measurements at Lotung Site," *Proceedings, EPRI/NRC/TPC Workshop on Seismic Soil - Structure Interaction Analysis Techniques Using Data From Lotung, Taiwan*, Vol. 2.

Shen, C.K. and H.Y. Yang (1990) "Phase III Soil Laboratory Testing Program Report - Lotung LSST Site," for EPRI, Department of Civil Engineering, University of California, Davis.

Wang, Z.L., Y.F. Dafalias, and C.K. Shen (1988) "Bounding Surface Hypoplasticity Model for Sands. I: Theoretical Formulation; II: Calibration and Application," Report, Dept. of Civil Engineering, University of California, Davis, CA.

Wang, Z.L., Y.F. Dafalias, and C.K. Shen (1990) "Bounding Surface Hypoplasticity Model," *Journal of Engineering Mechanics*, Vol. 116, No. 5, ASCE.

Wang, Z.L. (1990) "Bounding Surface Hypoplasticity Model for Granular Soils and Its Applications," Ph.D. Dissertation, Department of Civil Engineering, University of California, Davis

Wu, Wei-Teh, (1987) "Final Testing Report of Foundation Soils for Lotung Nuclear Power Plant Model - Phase II," for Taiwan Power Company, Civil Engineering Department, National Taiwan University.

Wu, Wei-Teh (1989) "Final Testing Report of Foundation for Lotung Nuclear Power Plant Model - Phase III," for Taiwan Power Company, Civil Engineering Department, National Taiwan University.